Influence of band state mixing on interband magnetotunnelling in broken-gap heterostructures

2002 J. Phys.: Condens. Matter 14 5003

(http://iopscience.iop.org/0953-8984/14/19/322)

INSTITUTE OF PHYSICS PUBLISHING JOURNAL OF PHYSICS: CONDENSED MATTER

J. Phys.: Condens. Matter **14** (2002) 5003–5016 PII: S0953-8984(02)31989-1

Influence of band state mixing on interband magnetotunnelling in broken-gap heterostructures

A Zakharova[1,2] **and K A Chao**[3]

[1] Physics Division, National Centre for Theoretical Sciences, Hsinchu, Taiwan, Republic of China
[2] Institute of Physics and Technology of the Russian Academy of Sciences, Nakhimovskii Avenue 34, Moscow 123098, Russia
[3] Department of Physics, Lund University, Sölvegutun 14A, S 233 62 Lund, Sweden

Received 18 December 2001, in final form 15 April 2002
Published 2 May 2002
Online at stacks.iop.org/JPhysCM/14/5003

Abstract

We investigate in detail the effect of electron and light- and heavy-hole state mixing on the transmission coefficients and current–voltage characteristics of interband tunnelling broken-gap heterostructures in the presence of a quantizing magnetic field perpendicular to the interfaces. Double-barrier and barrierless resonant tunnelling structures made from InAs, AlSb, and GaSb are considered. The multiband Burt envelope function theory and the cylindrical approximation are used to obtain analytical solutions for bulk dispersions, and wavefunctions in heterostructures are derived with the transfer matrix method. Taking into account the mixing of the states of different Landau-level indices at the interfaces due to the spin–orbit interaction, we have calculated the transmission coefficients for the coherent tunnelling transitions between the states of various Landau levels, as well as the corresponding tunnelling current components. We have shown that the mixing with the heavy-hole states results in additional peaks of the current density. The tunnelling processes in which the Landau-level index is not conserved may contribute significantly to these additional peaks.

1. Introduction

Since it was proposed [1,2] to investigate broken-gap heterostructures based on InAs, AlSb, and GaSb, such material systems have been studied extensively. In these heterostructures the InAs conduction band overlaps with the GaSb valence band, allowing interband transitions between the InAs conduction band states and the GaSb valence band states. Using this characteristic band alignment, new devices like interband tunnelling diodes and transistors [3–7], as well as the infrared detectors and laser diodes [8–12], have been made. The interband tunnelling exhibits a negative differential resistance with a high peak-to-valley current ratio larger than 20 at room temperature [3, 7], and a high peak current density [6] of about 10^5 A cm^{-2}.

0953-8984/02/195003+14$30.00

The absorption coefficient of the infrared detectors made from InAs/GaSb multiple quantum wells [8] has reached 6500 cm^{-1}. Recently, a high-efficiency interband cascade laser with a peak power of 4 W/facet was demonstrated [12].

In broken-gap heterostructures the coupling between electron, light-hole and heavy-hole states has been studied in connection to the quasiparticle spectrum and optical transitions in quantum wells and superlattices [13–15], cyclotron resonance and the quantum Hall effect [16, 17], and the interband tunnelling transport in resonant tunnelling structures (RTS) [18–20]. It was shown that the coupling between the InAs electron states and the GaSb heavy-hole quasibound states in InAs/AlSb/GaSb/AlSb/InAs RTS enhances the interband current considerably. This coupling significantly affects the interband resonant tunnelling times [21] and therefore the charge accumulation in the quantum well. This adds a further influence of the electron–hole coupling on the interband tunnelling current density [22].

Experiments on the interband magnetotunnelling in broken-gap RTS have shown unusual current–voltage (I–V) characteristics [23–26]. Additional peaks of the current density appear [23–25] when the magnetic field is perpendicular to interfaces, resulting from the interband tunnelling involving different Landau levels in the quantum well. When the magnetic field is parallel to interfaces, the current peak position in the I–V curve shifts with the field strength [26], allowing us to derive the subband dispersions. On the theory side, it was found [27] that the in-plane magnetic field can enhance the coupling between electron states and heavy-hole states, resulting in an increase of resonant tunnelling transport through the heavy-hole quasibound states. However, for the case of magnetic field applied perpendicular to interfaces, the role of electron–heavy-hole coupling in transport processes is much less understood. The first theoretical result on transmission coefficients was reported only recently [28]. In earlier studies on the I–V characteristics of InAs/AlSb/GaSb/AlSb/InAs RTS under a perpendicular magnetic field [29, 30], the heavy-hole states were neglected. This missing coupling with the heavy-hole states will be included in the present work.

We will use the envelope function theory of Burt [31] and the model described by Foreman [32] for zinc-blende structure materials. Both the intra- and inter-Landau-level transmission coefficients, and the interband tunnelling current through the light- and heavy-hole quasibound states in the well of a RTS will be calculated using the transfer matrix method. Due to the mixing of states belonging to different Landau levels caused by the spin–orbit interaction at interfaces, the inter-Landau-level processes can occur without scattering [30]. In this paper we will show the appearance of new peaks in the tunnelling current density due to the coupling of the electron and light-hole states to the heavy-hole states, and the inter-Landau-level processes may contribute considerably to the intensities of these peaks. Our results will provide a qualitative description of the measured I–V curves of the InAs/AlSb/GaSb/AlSb/InAs RTS [24] and the barrierless InAs/GaSb/InAs [25] structure under high pulsed magnetic fields up to 40 T.

2. Model description

We will study the InAs/AlSb/GaSb/AlSb/InAs double-barrier RTS and the barrierless InAs/GaSb/InAs structure grown along the ⟨100⟩ direction, which we define as the z-axis. The band diagrams are specified in figures 1(a) and (b). We start with the 8×8 $\boldsymbol{k} \cdot \boldsymbol{p}$ Hamiltonian [32] in the absence of a magnetic field. In the presence of a magnetic field with the associated vector potential $\boldsymbol{A}$, the momentum operators $\hat{k}_l = -\mathrm{i}\,\partial/\partial l$ with $l = x$, y, and z should be replaced by the canonical momentum operators $\hat{K}_l = -\mathrm{i}\,\partial/\partial l + |e|A_l/(\hbar c)$, where e is the electron charge and c the speed of light. To solve the eigenvalue problem, we will apply a unitary transformation [33] to the Hamiltonian such that at $\boldsymbol{K} = 0$ the 8×8 matrix

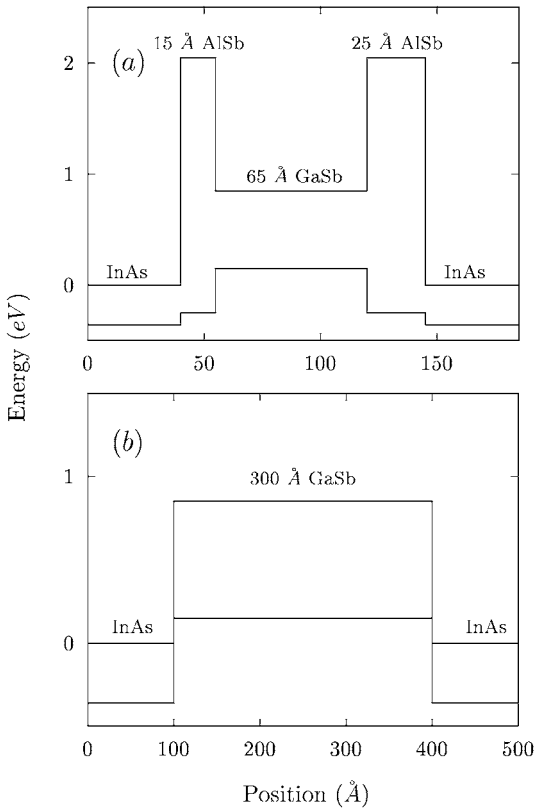

Figure 1. Conduction and valence band diagrams of the InAs/AlSb/GaSb/AlSb/InAs double-barrier RTS (panel (*a*)), and InAs/GaSb/InAs barrierless structure (panel (*b*)).

is diagonalized. Because of the formation of Landau levels, the theoretical analysis is very complicated. Since the split-off band lies far away from the energies of the tunnelling carriers, we will ignore the split-off band without any qualitative effect on our results. This simplification allows us to obtain analytical solutions for bulk dispersions, and then use them to calculate the transmission coefficients. If we define $\hat{K}_{\pm} = \mp \mathrm{i}(\hat{K}_x \pm \mathrm{i}\hat{K}_y)/\sqrt{2}$, the so-obtained 6×6 Hamiltonian $\hat{H}_K$, with the proper arrangement of canonical momentum operators and material parameters, can be expressed as

$$\hat{H}_K = \begin{pmatrix} \hat{H}_{+-} & \hat{H}_{--} \\ \hat{H}_{++} & \hat{H}_{-+} \end{pmatrix}, \tag{1}$$

with

$$\hat{H}_{\pm\mp} = \begin{pmatrix} \hat{H}_{cc} & \sqrt{2}\mathrm{i}P\hat{K}_z/\sqrt{3} & P\hat{K}_{\pm} \\ -\sqrt{2}\mathrm{i}P\hat{K}_z/\sqrt{3} & E_v(z) + \hat{G}_{\pm} & \hat{S}_{\pm} \\ P\hat{K}_{\mp} & \hat{S}_{\pm}^{\dagger} & E_v(z) + \hat{F}_{\pm} \end{pmatrix} \tag{2}$$

and

$$\hat{H}_{\pm\pm} = \begin{pmatrix} 0 & P\hat{K}_{\pm}/\sqrt{3} & 0 \\ P\hat{K}_{\pm}/\sqrt{3} & \hat{T}_{\pm} & \hat{R}_{\pm} \\ 0 & \hat{R}_{\pm} & 0 \end{pmatrix}, \tag{3}$$

where

$$\hat{G}_{\pm} = \frac{\hbar^2}{2m}[\hat{K}_+(\gamma_2 - \gamma_1)\hat{K}_- + \hat{K}_-(\gamma_2 - \gamma_1)\hat{K}_+ - \hat{K}_z(2\gamma_2 + \gamma_1)\hat{K}_z] \mp \tfrac{1}{6}(\hat{K}_+(N_+ - N_-)\hat{K}_- - \hat{K}_-(N_+ - N_-)\hat{K}_+), \tag{4}$$

$$\hat{F}_{\pm} = -\frac{\hbar^2}{2m}[\hat{K}_+(\gamma_2 + \gamma_1)\hat{K}_- + \hat{K}_-(\gamma_2 + \gamma_1)\hat{K}_+ - \hat{K}_z(2\gamma_2 - \gamma_1)\hat{K}_z] \mp \tfrac{1}{2}(\hat{K}_+(N_+ - N_-)\hat{K}_- - \hat{K}_-(N_+ - N_-)\hat{K}_+), \tag{5}$$

$$\hat{S}_{\pm} = -\frac{\mathrm{i}\sqrt{2}}{\sqrt{3}}(\hat{K}_z N_+ \hat{K}_{\pm} + \hat{K}_{\pm} N_- \hat{K}_z), \tag{6}$$

$$\hat{T}_{\pm} = -\frac{\mathrm{i}\sqrt{2}}{3}(\hat{K}_z(N_+ - N_-)\hat{K}_{\pm} - \hat{K}_{\pm}(N_+ - N_-)\hat{K}_z), \tag{7}$$

$$\hat{R}_{\pm} = -\frac{\hbar^2\sqrt{3}}{2m}[\hat{K}_+\gamma_2\hat{K}_+ + \hat{K}_-\gamma_2\hat{K}_-] \mp \frac{1}{2\sqrt{3}}(\hat{K}_- N \hat{K}_- - \hat{K}_+ N \hat{K}_+). \tag{8}$$

In the above equations,

$$\hat{H}_{cc} = E_c(z) + \hat{\boldsymbol{K}} A_c(z) \hat{\boldsymbol{K}}, \tag{9}$$

$E_c(z)$ is the conduction band edge, $E_v(z)$ is the valence band edge, $A_c(z)$ represents the effect of remote bands on the electron effective mass, m is the free-electron mass, and P is the interband momentum matrix element, which is supposed to be a constant value for the entire structure. N_+, N_-, and $N = N_+ + N_-$ are expressed in terms of the modified Luttinger parameters γ_1, γ_2, and γ_3 as

$$\begin{aligned} N_- &= -(\hbar^2/2m)(\gamma_1 - 2\gamma_2 + 1), \\ N_+ &= -(\hbar^2/2m)(6\gamma_3) - N_-. \end{aligned} \tag{10}$$

All Luttinger parameters are material dependent, so they are functions of z.

Now we will add to $\hat{H}_K$ the Zeeman term $\hat{H}_Z$ to arrive at the 6×6 Hamiltonian

$$\hat{H}_6 = \hat{H}_K + \hat{H}_Z. \tag{11}$$

For a magnetic field B along the z-axis, the elements $(\hat{H}_Z)_{ij}$ of $\hat{H}_Z$ are defined as $\mu_B g_0 \langle u_i | \hat{\boldsymbol{s}} \cdot \boldsymbol{B} | u_j \rangle = \mu_B g_0 \langle u_i | \hat{s}_z B | u_j \rangle$, where $g_0 = 2$, μ_B is the Bohr magneton, u_i is a basis function, and $\hat{\boldsymbol{s}}$ is the spin operator. The set of basis functions corresponding to the Hamiltonian $\hat{H}_6$ is given in the appendix. With respect to these basis functions, $\hat{H}_Z$ has the form

$$\hat{H}_Z = \mu_B B \begin{pmatrix} 1 & 0 & 0 & 0 & 0 & 0 \\ 0 & 1/3 & 0 & 0 & 0 & 0 \\ 0 & 0 & 1 & 0 & 0 & 0 \\ 0 & 0 & 0 & -1 & 0 & 0 \\ 0 & 0 & 0 & 0 & -1/3 & 0 \\ 0 & 0 & 0 & 0 & 0 & -1 \end{pmatrix}. \tag{12}$$

Then the envelope functions ψ_n of the entire heterostructure with abrupt interfaces satisfy the equations

$$\sum_l \hat{H}_{nl}\psi_l = E\psi_n, \qquad n = 1, 2, \ldots, 6, \tag{13}$$

with the eigenenergy E. The boundary conditions can be obtained by integrating equations (13) across an interface [31, 32].

3. Eigenvalue equations in heterostructures

We will use the cylindrical approximation, $\gamma_2 = \gamma_3$, as in [33]. To avoid unphysical spurious solutions, $A_c(z)$ in H_{cc} should be set to zero [32]. Because in the InAs conduction band the g-factor is much larger than g_0, the elements $(H_Z)_{11}$ and $(H_Z)_{44}$ in H_Z can be neglected. We choose the vector potential $A_y = Bx$ and $A_x = A_z = 0$. Consequently, we have $\hat{K}_x = -\mathrm{i}\,\partial/\partial x$, $\hat{K}_y = -\mathrm{i}\,\partial/\partial y + |e|Bx/\hbar c$, and $\hat{K}_z = -\mathrm{i}\,\partial/\partial z$.

With $A_c(z) = 0$, the conduction band envelope functions play a secondary role [32] and can be expressed in terms of the valence band envelope functions as

$$\psi_1 = (E - E_c)^{-1}(\sqrt{2}\mathrm{i}P\hat{k}_z\psi_2/\sqrt{3} + P\hat{K}_+\psi_3 + P\hat{K}_-\psi_5/\sqrt{3}), \tag{14}$$

$$\psi_4 = (E - E_c)^{-1}(\sqrt{2}\mathrm{i}P\hat{k}_z\psi_5/\sqrt{3} + P\hat{K}_-\psi_6 + P\hat{K}_+\psi_2/\sqrt{3}). \tag{15}$$

Then the eigenvalue equations reduce to the form

$$H_4\boldsymbol{F} = E\boldsymbol{F}, \tag{16}$$

where

$$\boldsymbol{F} = (\psi_2\psi_3\psi_5\psi_6)^{\mathrm{T}}. \tag{17}$$

The energy-dependent 4×4 Hamiltonian $\hat{H}_4$ is obtained from $\hat{H}_6$ by removing the rows and columns corresponding to the conduction band, and replacing N, N_+, γ_1, and $\gamma_2 = \gamma_3$ with

$$N' = N + P^2(E - E_c)^{-1}, \tag{18}$$

$$N'_+ = N_+ + P^2(E - E_c)^{-1}, \tag{19}$$

$$\gamma'_1 = \gamma_1 - E_p(3(E - E_c))^{-1}, \tag{20}$$

$$\gamma'_2 = \gamma'_3 = \gamma_2 - E_p(6(E - E_c))^{-1}, \tag{21}$$

where $E_p = 2mP^2/\hbar^2$.

The boundary conditions to be satisfied by the solutions of equation (16), and hence of equations (13), are derived by integrating equation (16) across an interface [32]. They ensure the continuity of the probability current density at an interface. Then, across interfaces both vector functions $\boldsymbol{F}$ and $\hat{H}_B\boldsymbol{F}$ are continuous, where

$$\hat{H}_B = \begin{pmatrix} GB & SB_+ & TB_- & 0 \\ CB_- & FB & 0 & 0 \\ TB_+ & 0 & GB & SB_- \\ 0 & 0 & CB_+ & FB \end{pmatrix}, \tag{22}$$

with elements

$$\begin{aligned} GB &= -\frac{\hbar^2}{2m}(2\gamma'_2 + \gamma'_1)\hat{k}_z, \\ FB &= \frac{\hbar^2}{2m}(2\gamma'_2 - \gamma'_1)\hat{k}_z, \\ SB_\pm &= \frac{\hbar^2}{m}\sqrt{6}\mathrm{i}\gamma'_2\hat{K}_\pm + \frac{\mathrm{i}\sqrt{2}}{\sqrt{3}}N_-\hat{K}_\pm, \\ CB_\pm &= \frac{\mathrm{i}\sqrt{2}}{\sqrt{3}}N_-\hat{K}_\pm, \\ TB_\pm &= 2\mathrm{i}\sqrt{2}\left(\frac{\hbar^2}{2m}\gamma'_2 + \frac{N_-}{3}\right)\hat{K}_\pm. \end{aligned} \tag{23}$$

4. Analytical solutions for bulk dispersions

Since $\gamma_2 = \gamma_3$, the solutions of equations (13) for a bulk material can be expressed in terms of a finite number of eigenstates of a free charged particle in a uniform magnetic field [33]. We define

$$\begin{aligned} &f_\nu(x') = \exp(-sx'^2/2)H_\nu(\sqrt{s}x'), && \nu \geqslant 0; \\ &f_\nu(x') = 0, && \nu < 0, \end{aligned} \tag{24}$$

where $H_\nu(\sqrt{s}x')$ is the Hermite polynomial and $x' = x - x_0$, with $x_0 = -k_y/s$ and $s = |e|B/\hbar c$. For $\nu \geqslant 0$, ν is just the Landau-level index and $f_\nu(x')$ is a harmonic oscillator function. Hence the multicomponent envelope functions have the form

$$\psi^{(n)} = \begin{pmatrix} C_1 f_n(x') \\ C_2 f_n(x') \\ C_3 f_{n-1}(x') \\ C_4 f_{n+1}(x') \\ C_5 f_{n+1}(x') \\ C_6 f_{n+2}(x') \end{pmatrix} \exp(\mathrm{i}k_y y + \mathrm{i}k_z z). \tag{25}$$

It is important to notice that an eigenstate $\psi^{(n)}$ with the quantum number n contains many components corresponding to different Landau levels with indices $\nu = n-1$, n, $n+1$, and $n+2$. Using the envelope functions ψ_2, ψ_3, ψ_5, and ψ_6 to construct the $\boldsymbol{F}$ in (17), and then substituting it into (16), we arrive at the equation for $\boldsymbol{C} = (C_2 C_3 C_5 C_6)^{\mathrm{T}}$:

$$\frac{\hbar^2}{2m}(B^{(2)}k_z^2 + B^{(1)}\mathrm{i}k_z + B^{(0)})\boldsymbol{C} = (E - E_v)\boldsymbol{C}. \tag{26}$$

The matrices $B^{(2)}$, $B^{(1)}$, and $B^{(0)}$ are

$$B^{(2)} = \begin{pmatrix} -(2\gamma_2' + \gamma_1') & 0 & 0 & 0 \\ 0 & 2\gamma_2' - \gamma_1' & 0 & 0 \\ 0 & 0 & -(2\gamma_2' + \gamma_1') & 0 \\ 0 & 0 & 0 & 2\gamma_2' - \gamma_1' \end{pmatrix}, \tag{27}$$

$$B^{(1)} = 2\sqrt{3}\gamma_2'\sqrt{s}\begin{pmatrix} 0 & 1 & 0 & 0 \\ -2n & 0 & 0 & 0 \\ 0 & 0 & 0 & 2(n+2) \\ 0 & 0 & -1 & 0 \end{pmatrix}, \tag{28}$$

$$B^{(0)} = s\begin{pmatrix} 2(n+1)\gamma_- - \frac{2}{3}(2\gamma_n + 1) & 0 & 0 & -4\sqrt{3}(n+1)(n+2)\gamma_2' \\ 0 & -2n\gamma_+ - 2\gamma_n & -4\sqrt{3}n(n+1)\gamma_2' & 0 \\ 0 & -\sqrt{3}\gamma_2' & 2(n+1)\gamma_- + \frac{2}{3}(2\gamma_n + 1) & 0 \\ -\sqrt{3}\gamma_2' & 0 & 0 & -2(n+2)\gamma_+ + 2\gamma_n \end{pmatrix}. \tag{29}$$

In the above equation, $\gamma_\pm = \gamma_2' \pm \gamma_1'$ and $\gamma_n = 2mN_-/\hbar^2$.

Then for quantum number $n \geqslant 1$, the equation for bulk dispersions can be expressed as

$$\begin{aligned} &\left[\left(B_{11}^{(2)}k_z^2 + B_{11}^{(0)} - \epsilon\right)\left(B_{22}^{(2)}k_z^2 + B_{22}^{(0)} - \epsilon\right) + k_z^2 B_{12}^{(1)}B_{21}^{(1)}\right] \\ &\quad \times \left[\left(B_{33}^{(2)}k_z^2 + B_{33}^{(0)} - \epsilon\right)\left(B_{44}^{(2)}k_z^2 + B_{44}^{(0)} - \epsilon\right) + k_z^2 B_{34}^{1}B_{43}^{1}\right] \\ &\quad + B_{41}^{(0)}B_{32}^{(0)}B_{23}^{(0)}B_{14}^{(0)} + B_{41}^{(0)}B_{12}^{(1)}B_{23}^{(0)}B_{34}^{(1)}k_z^2 + B_{14}^{(0)}B_{21}^{(1)}B_{32}^{(0)}B_{43}^{(1)}k_z^2 \\ &\quad - B_{41}^{(0)}B_{14}^{(0)}\left(B_{22}^{(2)}k_z^2 + B_{22}^{(0)} - \epsilon\right)\left(B_{33}^{(2)}k_z^2 + B_{33}^{(0)} - \epsilon\right) \\ &\quad - B_{23}^{(0)}B_{32}^{(0)}\left(B_{11}^{(2)}k_z^2 + B_{11}^{(0)} - \epsilon\right)\left(B_{44}^{(2)}k_z^2 + B_{44}^{(0)} - \epsilon\right) = 0, \end{aligned} \tag{30}$$

where $\epsilon = 2m(E - E_v)/\hbar^2$. This fourth-order equation in k_z^2 yields four bulk states. In each of these states the electron or the light-hole states of indices $\nu = n$ and $n + 1$ mix with the heavy-hole states of indices $\nu = n - 1$ and $n + 2$ with different spin orientations. This mixing is due to the off-diagonal terms in matrices $B^{(1)}$ and $B^{(0)}$ which are proportional to $\sqrt{B}$ and B, respectively.

For quantum number $n = 0$, $C_3 = 0$ because the corresponding function $f_{\nu=n-1}(x')$ is zero. Then the equation for the dispersion relations is third order in k_z^2:

$$\left[\left(B_{33}^{(2)}k_z^2 + B_{33}^{(0)} - \epsilon\right)\left(B_{44}^{(2)}k_z^2 + B_{44}^{(0)} - \epsilon\right) + k_z^2 B_{34}^{(1)} B_{43}^{(1)}\right] \times \left(B_{11}^{(2)}k_z^2 + B_{11}^{(0)} - \epsilon\right) - \left(B_{33}^{(2)}k_z^2 + B_{33}^{(0)} - \epsilon\right) B_{14}^{(0)} B_{41}^{(0)} = 0. \tag{31}$$

So, the dispersions of three bulk states can be obtained. In each of the corresponding states, the electron or the light-hole states of indices $\nu = n = 0$ and $\nu = n + 1 = 1$ with spins along and opposite to the magnetic field mix with the heavy-hole states of index $\nu = n + 2 = 2$ with spin $s_z \simeq -1/2$.

For the case $n = -1$, both $C_2 = 0$ and $C_3 = 0$ because $f_{\nu=n}(x') = 0$ and $f_{\nu=n-1}(x') = 0$. Hence, only two bulk states are mixed: the electron or light-hole states of index $\nu = n = 0$ and the heavy-hole states of index $\nu = n + 1 = 1$ with spins opposite to the magnetic field. The dispersions of these two states are given by

$$\left(B_{33}^{(2)}k_z^2 + B_{33}^{(0)} - \epsilon\right)\left(B_{44}^{(2)}k_z^2 + B_{44}^{(0)} - \epsilon\right) + k_z^2 B_{34}^{(1)} B_{43}^{(1)} = 0. \tag{32}$$

The last term in the above equation, which produces the mixing, is proportional to the magnetic field.

For quantum number $n = -2$ we have $C_2 = C_3 = C_5 = 0$, and the eigenfunction contains only one heavy-hole state of index $\nu = n + 2 = 0$ with spin $s_z = -1/2$. The corresponding dispersion is

$$B_{44}^{(2)}k_z^2 + B_{44}^{(0)} - \epsilon = 0. \tag{33}$$

Since this state does not mix with any other state, interband tunnelling through it cannot occur.

Equations (30)–(33) are up to the fourth order in k_z^2, and have solutions in the form $k_z^2 = \phi_i(E, n)$ [34], which define the dispersions of bulk states for all quantum numbers n. The corresponding envelope functions are given by (25), for which the vector $\boldsymbol{C} = (C_2 C_3 C_5 C_6)^{\mathrm{T}}$ is derived from equation (26). Using equations (14) and (15) the residual coefficients C_1 and C_4 can be expressed in terms of C_2, C_3, C_5, C_6 as

$$\begin{aligned} C_1 &= (E - E_c)^{-1}(\sqrt{2}\mathrm{i}Pk_zC_2/\sqrt{3} + P\sqrt{s}C_3/\sqrt{2} + 2(n+1)P\sqrt{s}C_5/\sqrt{6}), \\ C_4 &= (E - E_c)^{-1}(P\sqrt{s}C_2/\sqrt{6} + \sqrt{2}\mathrm{i}Pk_zC_5/\sqrt{3} + 2(n+2)P\sqrt{s}C_6/\sqrt{2}). \end{aligned} \tag{34}$$

5. Interband magnetotunnelling

We construct the wavefunctions in each layer of a heterostructure from all transmitted and reflected bulk states for a given energy and k_y. Then, using the boundary conditions, the solutions of equations (13) are obtained with the transfer matrix method. The detailed procedure of using the transfer matrix method to calculate wavefunctions within the framework of multiband envelope function approach is given in [35]. In accordance with the boundary conditions at the interfaces, the mixing of the states occurs only for a given quantum number n. Because of this, we can calculate the wavefunctions in a heterostructure separately for each quantum number n. For $n = -1$ the transfer matrix is 4×4 due to the mixing of two bulk states. For $n = 0$ and for $n \geqslant 1$, the transfer matrices are 6×6 and 8×8, respectively. The mixing of different states at the interfaces implies the possible interband transport processes in which the Landau-level index and the spin orientation can change, as described in [30].

After deriving the wavefunctions, the coefficient of transmission from the incident state l into the transmitted state r is given by [30]

$$T_{rl} = \left(\int \mathrm{d}x\ j_{zr}\right) \Big/ \left(\int \mathrm{d}x\ j_{zl}\right), \tag{35}$$

where j_{zl}, j_{zr} are the normal components of the incident and the transmitted probability current density, respectively. The expression for j_z is

$$j_z = \mathrm{Re}(\psi^\dagger \hat{j}_z \psi), \tag{36}$$

with the probability current density operator

$$\hat{j}_z = \hat{v}_z = \frac{\mathrm{i}}{\hbar}[\hat{H}_6 z - z\hat{H}_6] = \frac{1}{\hbar}\begin{pmatrix} \hat{v}_z^+ & 0 \\ 0 & \hat{v}_z^- \end{pmatrix}, \tag{37}$$

where $\hat{v}_z$ is the velocity operator and

$$\hat{v}_z^\pm = \begin{pmatrix} 0 & \sqrt{2}\mathrm{i}P/\sqrt{3} & 0 \\ -\sqrt{2}\mathrm{i}P/\sqrt{3} & -\hbar^2(2\gamma_2+\gamma_1)\hat{k}_z/m & \hbar^2\sqrt{6}\mathrm{i}\gamma_2\hat{K}_\pm/m \\ 0 & -\hbar^2\sqrt{6}\mathrm{i}\gamma_2\hat{K}_\mp/m & \hbar^2(2\gamma_2-\gamma_1)\hat{k}_z/m \end{pmatrix}. \tag{38}$$

Then, under a bias voltage V, the current density components j_{rl} for intra- and inter-Landau-level interband tunnelling processes can be calculated as [30]

$$j_{rl} = \frac{|e|s}{(2\pi)^2\hbar}\int \mathrm{d}E\ T_{rl}(E, V)(f_l(E) - f_r(E + |e|V)), \tag{39}$$

where f_l, f_r are the Fermi–Dirac occupation probabilities for the states to the left and to the right of the RTS. The total current density is the sum of all components j_{rl}.

6. Results and discussion

For our numerical calculation, we have taken from [36, 37] all band structure parameters and the heavy-hole effective masses in various layer materials. The light-hole effective masses are $0.026\,m$ for InAs, $0.052\,m$ for GaSb, and $0.12\,m$ for AlSb [38]. Using the bulk dispersions given in [21], the interband momentum matrix element and the modified Luttinger parameters were derived. We use $0.023\,m$ for the electron effective mass in InAs to calculate the interband momentum matrix element.

We will first present the results for the InAs/AlSb/GaSb/AlSb/InAs broken-gap double-barrier RTS. We set the GaSb well width at 65 Å, and the two AlSb barrier widths at 15 and 25 Å. The energy of an incident electron is measured from the InAs conduction band edge. The InAs contacts have bulk properties. Under an external magnetic field the electron bulk states are characterized by Landau-level indices, because simple one-band model is approximately valid near the conduction band edge.

We have calculated the transmission coefficients under a magnetic field $B = 17$ T. The results for a bias voltage $V = 0.05$ V are plotted in figure 2 versus the energy of an incident electron. For quantum number n larger than 1, the interband resonant tunnelling is forbidden by the selection rule. The curves 1 and 2 in panel (a) correspond to the quantum numbers $n = -1$ and 0, respectively. Curve 3 in panel (b) is for $n = 1$, and curve 4 corresponds to $n = 0$. The eigenenergies of both the incident electron in the InAs emitter and the transmitted electron in the InAs collector are Landau levels. Inside the double-barrier RTS, due to the off-diagonal terms in matrices $B^{(1)}$ and $B^{(0)}$, the bulk hole Landau states are mixed. On the other hand, the tunnelling processes corresponding to curves 1, 2, and 3 in figure 2 occur with the conservation of the Landau-level index. As a result, curve 1 describes the interband tunnelling

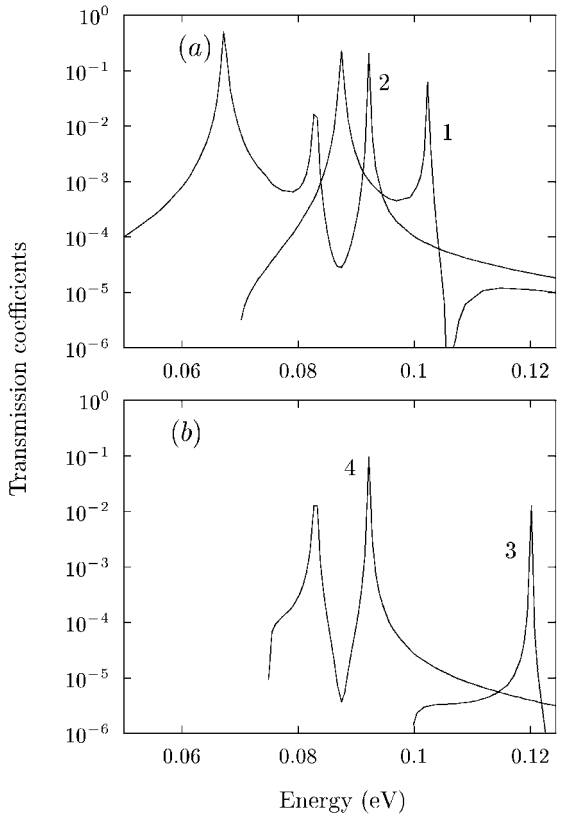

Figure 2. Transmission coefficients versus incident particle energy at the bias voltage $V = 0.05$ V and at $B = 17$ T for the double-barrier RTS.

between the states in the emitter with Landau-level index $\nu = 0$ and spin $s \simeq -1/2$ and the states in the collector with the same Landau-level index and spin. Curves 2 and 3 correspond to the transitions between the states with $s \simeq 1/2$ and indices $\nu = 0$ and 1, respectively. In this RTS under an applied bias, the spin-flip processes from the states with Landau-level index $\nu = 0$ and $s \simeq 1/2$ into the states with Landau-level index $\nu = 1$ are also allowed. Curve 4 represents these spin-flip processes with the change of the Landau-level index from $\nu = 0$ to 1. The probability of inter-Landau-level transitions, due to the mixing of the different states at interfaces caused by the spin–orbit interaction [30], is significant.

To identify the transport processes which are associated with all these peaks in figure 2, we have plotted the peak positions as functions of the applied magnetic field strength. The results for bias voltage $V = 0.05$ V are shown in figure 3, with panel (a) for quantum number $n = -1$, panel (b) for quantum number $n = 0$, and panel (c) for quantum number $n = 1$. At the extremely weak magnetic field $B \simeq 0$, at normal incidence, there is no mixing between the electron and the heavy-hole states. Therefore, the only resonant tunnelling process is through the light-hole quasibound state of the first space-quantized subband in the well. This state is labelled as LH_1. With a finite magnetic field strength, due to the mixing of the electron and the light-hole states with the heavy-hole states, there exist resonant tunnelling processes involving the heavy-hole states of the first and the second space-quantized subbands, which are labelled, respectively as HH_1 and HH_2. Each LH_1 peak for $n > -1$ and each HH_1 or HH_2

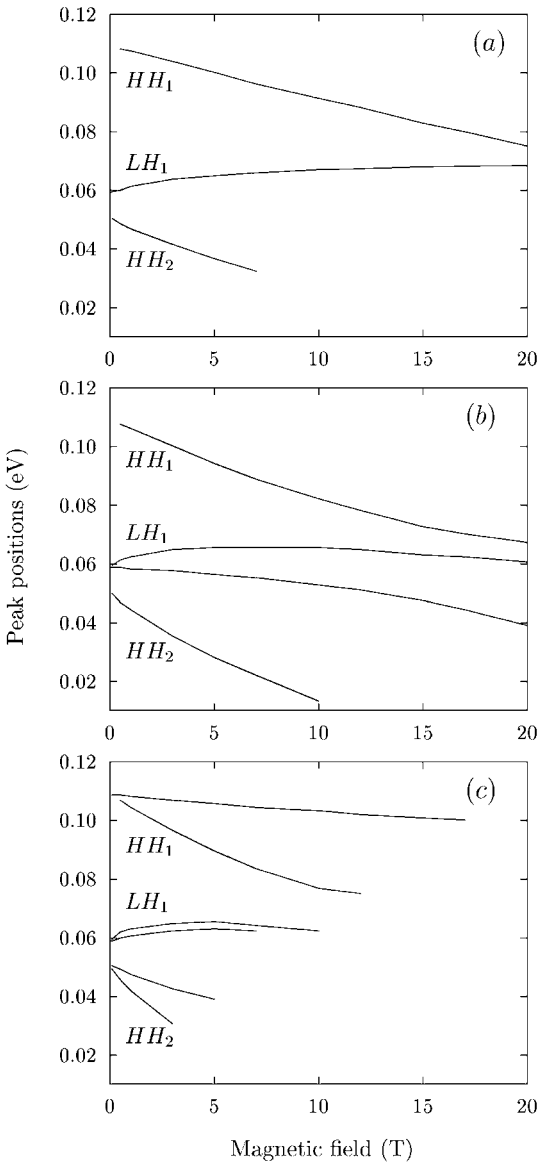

Figure 3. Positions of the transmission coefficient peaks versus the magnetic field for the double-barrier RTS at the bias voltage $V = 0.05$ V.

peak for $n > 0$ is split into two peaks due to the formation of Landau levels. Via the analysis of figure 3, we conclude that the two peaks in curve 1 of figure 2 mark the transitions through the mixed HH_1 state and the LH_1 state with spin opposite to the magnetic field direction, and with Landau-level indices $\nu = 1$ and 0. In figure 2, the three peaks in curve 2 and the two peaks in curve 4 are due to the resonant tunnelling through the mixed HH_1 state with the Landau-level index $\nu = 2$ and spin opposite to the magnetic field direction, as well as the resonant tunnelling through the LH_1 states with Landau-level indices $\nu = 0$ and 1, and with spins directed along and opposite to the magnetic field direction. The peak in curve 3 of figure 2 corresponds to the transitions through the HH_1 states.

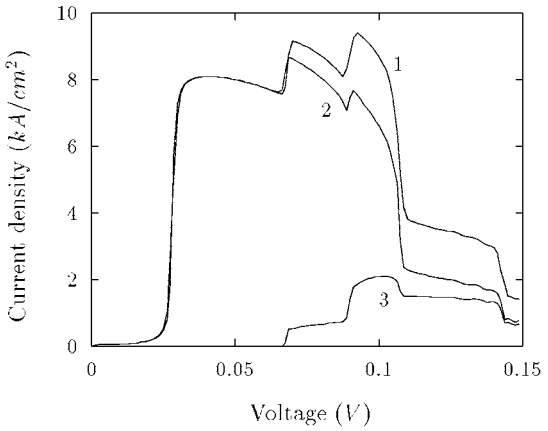

Figure 4. Total current density (curve 1) and current density components (curves 2 and 3) versus the bias voltage for the double-barrier RTS. The magnetic field is $B = 17$ T.

Figure 4 shows the calculated current density through an InAs/AlSb/GaSb/AlSb/InAs RTS under a magnetic field of 17 T at the temperature 1.5 K. The donor concentration in each InAs contact is $n_D = 10^{17}$ cm^{-3}. In this case the only interband transition is originated from the states of the lowest Landau level with $s \simeq 1/2$. Curve 1 is for the total current density, in which the three broad maxima are caused by the three resonant tunnelling peaks in curve 2 of figure 2. Such maxima of current density were observed experimentally [24]. The total current density has two contributions. One is from the transport process which conserves the Landau-level index (curve 2), and the other does not conserve the Landau-level index (curve 3). At large bias voltage, both contributions are important.

Next we present our calculated results for the barrierless InAs/GaSb/InAs structure with a 300 Å GaSb layer. The donor concentration in each InAs contact is $n_D = 10^{17}$ cm^{-3}. The parameters for this structure are taken from [25]. The I–V curve is shown in figure 5 for an applied magnetic field $B = 30$ T at the temperature 4.2 K. While the spin-flip processes with the changing Landau-level index are noticeable at lower magnetic fields, at such a high magnetic field as $B = 30$ T the spin-flip processes have a very weak effect on the total current which is plotted in figure 5. The current density oscillations with increasing applied bias are caused by the interband resonant transitions through various mixed states. Such oscillating behaviour was observed experimentally [25]. Furthermore, we obtained the result that the main peak position shifts toward lower voltage with increasing magnetic field. This was also observed in experiments [25].

From our calculation we found that the dominating interband transitions are from the states in the emitting InAs contact with Landau-level index $\nu = 0$ and spin $s \simeq 1/2$ to the similar states in the collecting InAs contact. The transmission coefficients for these dominating transitions are shown in figure 6 for a bias of 0.05 V, with panel (a) for $B = 0.01$ T and panel (b) for $B = 30$ T. For the weak magnetic field of 0.01 T, the interband transitions are through the light-hole states. The number of peaks increases with the magnetic field, because of the formation of the Landau levels as well as the appearance of the heavy-hole peaks. When the field strength is very high, all quasibound states are strongly mixed, and it becomes very difficult to identity the origin of the peaks.

We should mention that our theoretical analysis explains qualitatively the origin of the multiple current peaks and the tunnelling mechanism, although our approach does not predict the precise number of current peaks, the accurate bias voltage values at which these peaks

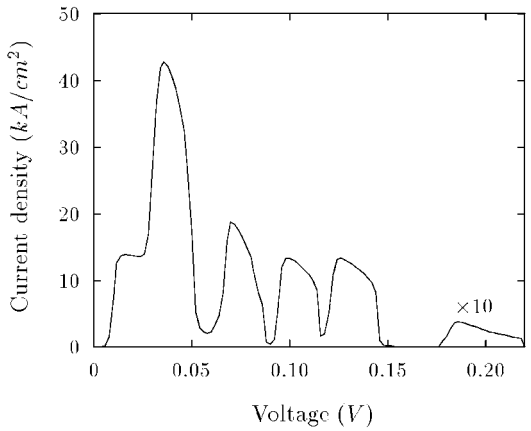

Figure 5. The I–V characteristic of the InAs/GaSb/InAs barrierless structure with a 300 Å GaSb quantum well under the magnetic field $B = 30$ T.

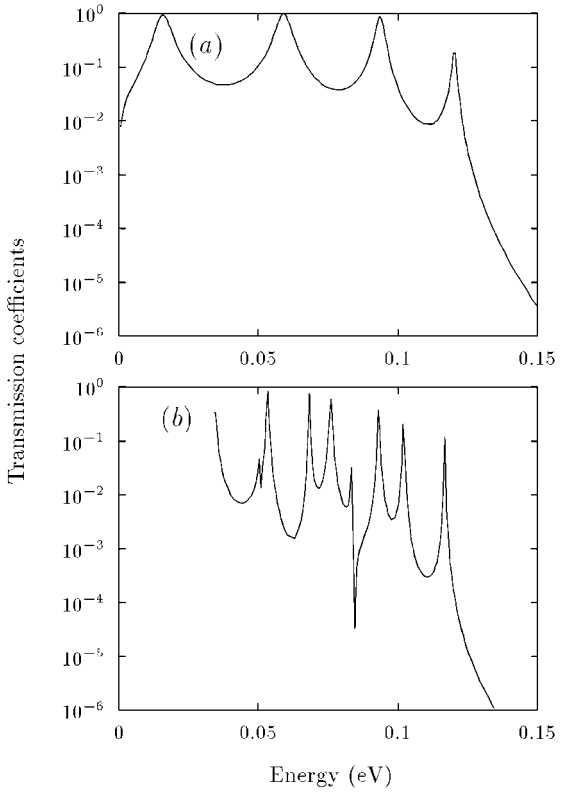

Figure 6. Transmission coefficients versus incident particle energy in the InAs/GaSb/InAs barrierless structure at the bias voltage $V = 0.05$ V. Panel (a) is for the magnetic field $B = 0.01$ T, and panel (b) is for the magnetic field $B = 30$ T.

appear, or the peak-to-valley current ratios. The experimentally observed valley current densities and the bias voltages for current peaks are larger than those shown in figure 5. Also, only three current peaks are detected [25]. The reason for the discrepancy between theory and

experiment is the neglect in our calculation of the scattering-assisted processes, band bending, and charge accumulation. It is clear that the scattering-assisted processes enhance the valley current but suppress the resonant tunnelling, and the other two effects modify the shape of the I–V curve. The band bending causes a shift in the current peak toward the higher bias voltage. The downward band bending in the emitting contact and the upward band bending in the quantum well also produce charge accumulation in both the emitting contact and the quantum well, which influence the band bending self-consistently. As a result, there is a decrease of the overlap between the valence band of the GaSb quantum well and the conduction band of the InAs emitting contact. This reduces the number of quasibound states in the well, and hence the number of resonant tunnelling peaks as observed experimentally. A self-consistent calculation is required to clarify all relevant details.

7. Conclusions

In summary, we have studied the influence of the coupling between the electron, the light-hole, and the heavy-hole states on the interband resonant tunnelling in broken-gap heterostructures under a quantizing magnetic field perpendicular to the interfaces. We found additional peaks in the transmission coefficients for the intra-Landau-level and inter-Landau-level tunnelling, as well as in the corresponding current density components. These additional peaks are caused by the resonant transitions through the mixed light-hole and heavy-hole quasibound states in the well with different Landau-level indices. The number of peaks is increased when the heavy-hole states are taken into account. As a result, several peaks appear in the I–V characteristics of both the double-barrier RTS and the barrierless structure. The transport processes, for which the Landau-level index changes, make a significant contribution to some of these peaks.

Acknowledgment

AZ thanks the National Science Council of the Republic of China (Taiwan) for partial financial support.

Appendix A

The basis functions used in the present work are

$$u_1 = |\mathrm{s}_{1/2,1/2}\rangle = |\mathrm{iS}\uparrow\rangle, \tag{A.1}$$

$$u_2 = |\mathrm{p}_{3/2,1/2}\rangle = (2/3)^{1/2}|\mathrm{p}_0\uparrow\rangle + (1/3)^{1/2}|\mathrm{p}_+\downarrow\rangle, \tag{A.2}$$

$$u_3 = |\mathrm{p}_{3/2,3/2}\rangle = |\mathrm{p}_+\uparrow\rangle, \tag{A.3}$$

$$u_4 = |\mathrm{s}_{1/2,-1/2}\rangle = |\mathrm{iS}\downarrow\rangle, \tag{A.4}$$

$$u_5 = |\mathrm{p}_{3/2,-1/2}\rangle = (2/3)^{1/2}|\mathrm{p}_0\downarrow\rangle + (1/3)^{1/2}|\mathrm{p}_-\uparrow\rangle, \tag{A.5}$$

$$u_6 = |\mathrm{p}_{3/2,-3/2}\rangle = |\mathrm{p}_-\downarrow\rangle, \tag{A.6}$$

where $|\mathrm{p}_0\rangle = \mathrm{i}|Z\rangle$, $|\mathrm{p}_\pm\rangle = \mp\mathrm{i}|X \pm \mathrm{i}Y\rangle/\sqrt{2}$, $|\mathrm{s}_{1/2,\pm1/2}\rangle$ are the electron states, $|\mathrm{p}_{3/2,\pm3/2}\rangle$ are the heavy-hole states, and $|\mathrm{p}_{3/2,\pm1/2}\rangle$ are the light-hole states.

References

[1] Esaki L, Chang L L and Mendez E E 1981 *Japan. J. Appl. Phys.* **20** L529
[2] Mendez E E, Chang L L and Esaki L 1982 *Surf. Sci.* **113** 474
[3] Södeström J R, Chow D H and McGill T C 1989 *Appl. Phys. Lett.* **55** 1094

[4] Luo L F, Beresford R and Wang W I 1989 *Appl. Phys. Lett.* **55** 2023
[5] Taira K, Hase I and Kawai K 1989 *Electron. Lett.* **25** 1708
[6] Ting D Z-Y, Collins D A, Yu E T, Chow D H and McGill T C 1990 *Appl. Phys. Lett.* **57** 1257
[7] Houng M P, Wang Y H, Shen S L, Chen J F and Cho A Y 1992 *Appl. Phys. Lett.* **60** 713
[8] Katz J, Zhang Y and Wang W I 1993 *Appl. Phys. Lett.* **62** 609
[9] Jenner C, Corbin E, Adderley B M and Jaros M 1998 *Semicond. Sci. Technol.* **13** 359
[10] Lin C-H, Yang R Q, Zhang D, Murry S L, Pei S S, Allerma A A and Kurtz S R 1997 *Electron. Lett.* **33** 598
[11] Yang B H, Zhang D, Yang R Q, Lin C-H, Murry S L and Pei S S 1998 *Appl. Phys. Lett.* **72** 2220
[12] Bradshaw J L, Yang R Q, Bruno J D, Pham J T and Wortman D E 1999 *Appl. Phys. Lett.* **75** 2220
[13] Altarelli M 1983 *Phys. Rev.* B **28** 842
[14] Wang L-W, Wei S H, Mattila T, Zunger A, Vurgaftman I and Meyer J R 1999 *Phys. Rev.* B **60** 5590
[15] Halvorsen E, Galperin Y and Chao K A 2000 *Phys. Rev.* B **61** 16 743
[16] Altarelli M, Maan J C, Chang L L and Esaki L 1987 *Phys. Rev.* B **35** R9867
[17] Vasilyev Yu, Suchalkin S, von Klitzing K, Meltser B, Ivanov S and Kop'ev P 1999 *Phys. Rev.* B **60** 10 636
[18] Ting D Z-Y, Yu E T and McGill T C 1992 *Phys. Rev.* B **45** 3583
[19] Kiledjin M S, Schulman J N, Wang K L and Rousseau K V 1992 *Phys. Rev.* B **46** 16 012
[20] Davidovich M A, Anda E V, Tejedor C and Platero G 1993 *Phys. Rev.* B **47** 4475
[21] Zakharova A 1998 *Semicond. Sci. Technol.* **13** 569
[22] Lapushkin I, Zakharova A, Gergel V, Goronkin H and Tehrani S 1997 *J. Appl. Phys.* **82** 2421
[23] Mendez E E, Ohno H, Esaki L and Wang W I 1991 *Phys. Rev.* B **43** 5196
[24] Mendez E E, Ohno H, Esaki L and Wang W I 1991 *Resonant Tunneling in Semiconductors. Physics and Applications (NATO ASI Series B: Physics, vol 277)* ed L L Chang, E E Mendez and C Tejedor (Dordrecht: Kluwer) p 51
[25] Takamasu T, Miura N, Taira K, Funato K and Kawai H 1992 *Surf. Sci.* **263** 217
[26] Marquardt R R, Collins D A, Liu Y X, Ting D Z-Y and McGill T C 1996 *Phys. Rev.* B **53** 13 624
[27] Liu Y X, Marquardt R R, Ting D Z-Y and McGill T C 1997 *Phys. Rev.* B **55** 7073
[28] Zakharova A 2000 *Solid State Commun.* **113** 599
[29] Davidovich M A 1995 *J. Appl. Phys.* **78** 5467
[30] Zakharova A 1999 *J. Phys.: Condens. Matter* **11** 4675
[31] Burt M G 1992 *J. Phys.: Condens. Matter* **4** 6651
[32] Foreman B A 1997 *Phys. Rev.* B **56** R12 748
[33] Wu G-Y, McGill T C, Mailhiot C and Smith D L 1989 *Phys. Rev.* B **39** 6060
[34] Korn G A and Korn T M 1968 *Mathematical Handbook* (New York: McGraw-Hill) ch 1
[35] Wessel R and Altarelli M 1989 *Phys. Rev.* B **39** 12 802
[36] Lapushkin I, Zakharova A and Gergel V 1999 *Semicond. Sci. Technol.* **14** 731
[37] Ryzhii V and Zakharova A 1993 *Semicond. Sci. Technol.* **8** 377
[38] Gantmakher V F and Levinson I B 1984 *Rasseyanie Nositelei v Metallakh i Poluprovodnikakh* (Moscow: Nauka)